Inorganic Chemistry

ARTICLE

pubs.acs.org/IC

Phase Relations and Crystal Structure of τ_6-$Ti_2(Ti_{0.16}Ni_{0.43}Al_{0.41})_3$

Atta U. Khan,[†] A. Grytsiv,[†] X. Yan,[†] P. Rogl,*[,†] A. Saccone,[‡] V. Pomjakushin,[§] and G. Giester[∥]

[†]Institute of Physical Chemistry, University of Vienna, Währingerstrasse 42, A-1090 Wien, Austria

[‡]Dipartimento di Chimica e Chimica Industriale, Università di Genova, Sezione di Chimica Inorganica e Metallurgia, Via Dodecaneso 31, I-16146 Genova, Italy

[§]Laboratorium für Neutronenstreuung, ETHZ & PSI, CH-5232 Villigen PSI, Switzerland

[∥]Institute of Mineralogy and Crystallography, University of Vienna, Althanstrasse 14, A-1090 Wien, Austria

ABSTRACT: $Ti_2(Ti_{0.16}Ni_{0.43}Al_{0.41})_3$ is a novel compound (labeled as τ_6) in the Ti-rich region of the Ti−Ni−Al system in a limited temperature range 870 < T < 980 °C. The structure of τ_6-$Ti_2(Ti,Ni,Al)_3$ was solved from a combined analysis of X-ray single crystal and neutron powder diffracton data (space group $C2/m$, a = 1.85383(7) nm, b = 0.49970(2) nm, c = 0.81511(3) nm, and β = 99.597(3)°). τ_6-$Ti_2(Ti,Ni,Al)_3$ as a variant of the $V_2(Co_{0.57}Si_{0.43})_3$-type is a combination of slabs of the $MgZn_2$-Laves type and slabs of the Zr_4Al_3-type forming a tetrahedrally close-packed Frank−Kasper structure with pentagon−triangle main layers. Titanium atoms occupy the vanadium sites, but Ti/Ni/Al atoms randomly share the (Co/Si) sites of $V_2(Co_{0.57}Si_{0.43})_3$. Although τ_6 shows a random replacement on 6 of the 11 atom sites, it has no significant homogeneity range (~1 at. %). The composition of τ_6 changes slightly with temperature. DSC/DTA runs (1 K/min) were not sufficient to define proper reaction temperatures due to slow reaction kinetics. Therefore, phase equilibria related to τ_6 were derived from X-ray powder diffraction in combination with EPMA on alloys, which were annealed at carefully set temperatures and quenched. τ_6 forms from a peritectoid reaction η-$(Ti,Al)_2Ni + \tau_3 + \alpha_2 \leftrightarrow \tau_6$ at 980 °C and decomposes in a eutectoid reaction $\tau_6 \leftrightarrow \eta + \tau_4 + \alpha_2$ at 870 °C. Both reactions involve the η-$(Ti,Al)_2Ni$ phase, for which the atom distribution was derived from X-ray single crystal intensity data, revealing Ti/Al randomly sharing the 48f- and 16c-positions in space group $Fd\bar{3}m$ (Ti_2Ni-type, a = 1.12543(3) nm). There was no residual electron density at the octahedral centers of the crystal structure ruling out impurity stabilization. Phase equilibria involving the τ_6 phase have been established for various temperatures (T = 865, 900, 925, 950, 975 °C, and subsolidus). The reaction isotherms concerning the τ_6 phase have been established and are summarized in a Schultz−Scheil diagram.

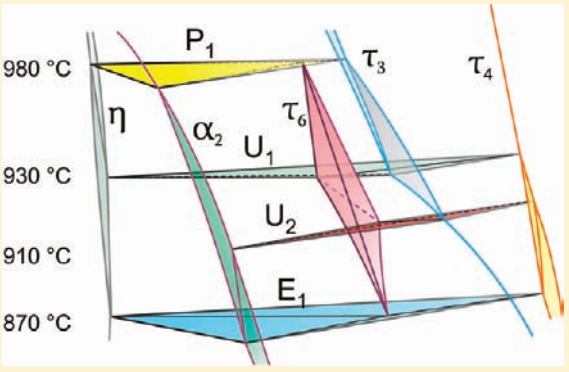

1. INTRODUCTION

Materials design of Ti_3Al- and TiAl-based high strength alloys involving third metal components essentially depends on a detailed knowledge of the temperature and solute dependent solubility limits as well as on the chemical and crystallographic nature of precipitates. Low-temperature brittleness has so far restricted utilization of titanium aluminides and requests further improvement of mechanical properties. In this respect, group-VIII elements as alloy constituents are of interest and among them particularly nickel because it can enhance oxidation resistance and tensile strength of Ti−Al alloys.[1]

Although several research teams have investigated the Ti−Ni−Al system, different phase constitution has been presented.[2−10] For details, the reader may be referred to recent assessments of phase diagram data by Raghavan[11,12] and by Schuster.[13] Thermodynamic calculations of the Ti−Ni−Al system were performed by three different groups.[10,14,15] In our recent reinvestigation,[16] two four-phase reactions have been elucidated, which have solved some of the hitherto puzzling data: (i) NiAl + τ_3-TiNiAl (Laves phase) ↔ τ_2-$TiNiAl_2$ + τ_4-$TiNi_2Al$ (Heusler-phase) at 925 °C ± 15 °C and (ii) τ_3-TiNiAl + τ_1-Ti_3NiAl_8 ($AuCu_3$-type) ↔ $TiAl_2$ + τ_2-$TiNiAl_2$ at 990 °C ± 15 °C. Furthermore, we confirmed the three-phase field τ_4 + α_2-Ti_3Al + τ_3, as reported at 900 °C by Huneau et al.,[7] while Schuster et al.[10] claimed a four-phase reaction $\{Ti,Al\}_2Ni + \tau_3 \leftrightarrow \alpha_2 + \tau_4$ at 876 ± 2 °C. For the Ti-rich region, we confirmed the findings of Grytsiv et al.[17] on a hitherto unknown phase τ_6 (near "Ti_2NiAl" ($Ti_{47-49}Ni_{27}Al_{26-24}$), which at that time was named τ_5). In the meantime, another phase in the Al-rich corner "$Ti_{15}Ni_{20}Al_{65}$" was labeled as τ_5.[13] In order to reduce confusion, we will keep the Al-rich phase as τ_5 and will label the Ti-rich phase reported by Grytsiv et al.[17] as τ_6. Because until now neither phase equilibria data involving the τ_6-phase nor crystal structure data have been published for τ_6, the current investigation was designed to provide this information including a reinvestigation of the structure of $(Ti,Al)_2Ni$ on the basis of X-ray single crystal (XSC) data. Although atom distribution in η-$(Ti_{0.81}Al_{0.19})_2Ni$ has been defined from X-ray Rietveld powder refinement,[18] single crystal data were used to derive high precision

Received: February 4, 2011
Published: April 14, 2011

Table 1. X-ray Single Crystal Data for τ_6-$Ti_2(Ti_{0.16}Ni_{0.43}Al_{0.41})_3$[a]

param/diff. technique	XSC	NPD	XRD
composition from EPMA (at. %)	$Ti_{50}Ni_{26.4}Al_{23.6}$	$Ti_{48.6}Ni_{27.3}Al_{24.1}$	$Ti_{48.6}Ni_{27.3}Al_{24.1}$
composition from refinement (at. %)	$Ti_{49.5}Ni_{26.1}Al_{24.4}$	$Ti_{49.0}Ni_{27.2}Al_{23.8}$	$Ti_{49.0}Ni_{27.2}Al_{23.8}$
formula from refinement	$Ti_{2.48}Ni_{1.30}Al_{1.22}$ = $Ti_2(Ti_{0.16}Ni_{0.43}Al_{0.41})_3$	$Ti_{2.45}Ni_{1.36}Al_{1.19}$ = $Ti_2(Ti_{0.15}Ni_{0.45}Al_{0.40})_3$	$Ti_{2.45}Ni_{1.36}Al_{1.19}$ = $Ti_2(Ti_{0.15}Ni_{0.45}Al_{0.40})_3$
radiation, λ (nm)	Mo Kα = 0.071 069	λ_n = 0.188 57	Cu Kα_1 = 0.154 056
a (nm)	1.853 83(7)	1.846 68(9)	1.846 85(3)
b (nm)	0.499 70(2)	0.498 95(3)	0.498 90(1)
c (nm)	0.815 11(3)	0.814 11(4)	0.813 80(1)
β (deg)	99.597(3)	99.541(4)	99.560(1)
V (nm^3)	0.744 52	0.750 12	0.749 82
reflns in refinement	1185 > 4$\sigma(F_o)$ of 1888	529	501
mosaicity	0.45		
no. of variables	89	54	54
$R_F = \Sigma\|F^o - F_c\|/\Sigma F_o$		0.055	0.036
$R_I = \Sigma\|I^o - I_c\|/\Sigma I_o$		0.034	0.043
$R_{wP} = [\Sigma w_i\|y_{oi} - y_{ci}\|^2/\Sigma w_i\|y_{oi}\|^2]^{1/2}$		0.117	0.065
$R_P = \Sigma\|y_{oi} - y_{ci}\|/\Sigma\|y_{oi}\|$		0.097	0.072
$R_e = [(N - P + C)/\Sigma w_i {y_{0i}}^2]^{1/2}$		0.012	0.009
$\chi^2 = (R_{wP}/R_e)^2$		8.00	4.82
$R_F{}^2 = \Sigma\|F_o{}^2 - F_c{}^2\|/\Sigma {F_o}^2$	0.0375		
R_{Int}	0.075		
wR2	0.086		
GOF	1.047		
extinction (Zachariasen)	0.0004(1)		
residual density e$^-$/Å^3, max; min	1.40; −1.35		
atom parameters			
Ti1 in 4i (x, 0, z); x, z	0.285 42(5), 0.080 03(10)	0.2859(3), 0.0771(7)	
U_{11}, U_{22}, U_{33}	0.0127(4), 0.0111(4), 0.0129(4)	B_{iso} = 0.41(3)	
$U_{23} = U_{12} = 0$, U_{13}	0.0009(3)		
Ti2 in 4i (x, 0, z); x, z	0.551 63(4), 0.360 02(10)	0.5478(3), 0.3684(7)	
U_{11}, U_{22}, U_{33}	0.0131(4), 0.0115(4), 0.0135(4)	B_{iso} = 0.87(2)	
$U_{23} = U_{12} = 0$, U_{13}	0.0025(3)		
Ti3 in 4i (x, 0, z); x, z	0.289 15(4), 0.452 88(10)	0.2917(3), 0.4533(7)	
U_{11}, U_{22}, U_{33}	0.0137(4), 0.0110(4), 0.0127(4)	B_{iso} = 0.67(2)	
$U_{23} = U_{12} = 0$, U_{13}	0.0031(3)		
Ti4 in 4i (x, 0, z); x, z	0.023 58(4), 0.168 84(10)	0.02754(3), 0.1767(6)	
U_{11}, U_{22}, U_{33}	0.0132(4), 0.0109(4), 0.0114(4)	B_{iso} = 0.84(2)	
$U_{23} = U_{12} = 0$, U_{13}	0.0026(3)		
Ti5 in 4i (x, 0, z); x, z	0.434 75(4), 0.019 61(10)	0.4316(3), 0.0153(6)	
U_{11}, U_{22}, U_{33}	0.0129(4), 0.0128(4), 0.0163(4)	B_{iso} = 0.73(2)	
$U_{23} = U_{12} = 0$, U_{13}	0.0038(3)		
M1 in 4i (x, 0, z); occ	0.073(1)Ti + 0.462Ni + 0.465Al	0.073(1)Ti + 0.462Ni + 0.465Al	
x, z	0.868 91(4), 0.043 77(10)	0.8706(3), 0.0446(7)	
U_{11}, U_{22}, U_{33}	0.0128(4), 0.0110(4), 0.0128(4)	B_{iso} = 0.43(1)	
$U_{23} = U_{12} = 0$, U_{13}	0.0022(3)		
M2 in 8j (x, y, z); occ	0.136(1)Ti + 0.421Ni + 0.443Al	0.110(1)Ti + 0.482Ni + 0.407Al	
x, y, z	0.168 74(3), 0.255 31(11), 0.218 56(7)	0.1685(2), 0.2600(8), 0.2202(4)	
U_{11}, U_{22}, U_{33}	0.0134(3), 0.0083(3), 0.0112(3)	B_{iso} = 0.31(1)	
U_{23}, U_{13}, U_{12}	−0.0003(2), 0.0013(2), −0.0017(2)		
M3 in 8j (x, y, z); occ	0.164(1)Ti + 0.507Ni + 0.329Al	0.165(1)Ti + 0.503Ni + 0.332Al	
x, y, z	0.407 63(3), 0.235 86(11), 0.309 69(6)	0.4060(2), 0.2343(6), 0.3073(4)	
U_{11}, U_{22}, U_{33}	0.0134 (3), 0.0105(3), 0.0121(3)	B_{iso} = 0.81(2)	
U_{23}, U_{13}, U_{12}	−0.0012(2), 0.0022 (2), −0.0002(2)		
M4 in 2c (0, 0, $^1/_2$); occ	0.262(2)Ti + 0.440Ni + 0.298Al	0.248(2)Ti + 0.496Ni + 0.256Al	
U_{11}, U_{22}, U_{33}	0.0118(6), 0.0133(6), 0.0128(6)	B_{iso} = 0.26(3)	
$U_{23} = U_{12} = 0$, U_{13}	0.0027(4)		
M5 in 4i (x, 0, z); occ	0.151(2)Ti + 0.488Ni + 0.361Al	0.150(2)Ti + 0.465Ni + 0.385Al	
x, z	0.133 48(4), 0.451 00(10)	0.1295(3), 0.4552(7)	
U_{11}, U_{22}, U_{33}	0.0125(4), 0.0138(4), 0.0136(4)	B_{iso} = 0.73(3)	
$U_{23} = U_{12} = 0$, U_{13}	0.0013(3)		
M6 in 4i (x, 0, z); occ	0.238(1)Ti + 0.237Ni + 0.525Al	0.232(1)Ti + 0.258Ni + 0.510Al	
x, z	0.213 32(5), 0.735 33(11)	0.2158(4), 0.7340(8)	
U_{11}, U_{22}, U_{33}	0.0124(4), 0.0144(5), 0.0133(5)	B_{iso} = 0.26(3)	
$U_{23} = U_{12} = 0$, U_{13}	0.0024(4)		

[a] Space group $C2/m$, No. 12 ($V_2(Co_{0.57}Si_{0.43})_3$ structure type) standardized with program *Structure Tidy*.[24] Data collection details: XSC; 2° ≤ 2Θ ≤ 72.05°; ω-scans, scan width 2°; 150 s/frame, NPD; 3.85° ≤ 2Θ ≤ 164.8° and XRD; 8° ≤ 2Θ ≤100°; B_{iso} (10^2 nm^2).

dx.doi.org/10.1021/ic200245m |*Inorg. Chem.* 2011, 50, 4537–4547

Table 2. Interatomic Distances (nm) for τ_6 Taken from XSC Refinement (Upper Right Column), Standard Deviation ≤ 0.0001 nm

Ti1−	2M1	0.2871		2M3	0.2916		1Ti1	0.3015
CN = 16	1Ti5	0.2891		2M2	0.2944	M3−	1M3	0.2357
	3M2	0.2897		2Ti2	0.2944	CN = 12	1M4	0.2489
	1M6	0.2902		2Ti5	0.3098		1M1	0.2537
	3M6	0.2915		2Ti5	0.3125		1M5	0.2537
	2M3	0.2935	Ti5−	1Ti5	0.2494		1M6	0.2575
	1M1	0.2980	CN = 14	2M3	0.2761		1M3	0.2640
	2Ti1	0.3015		2M2	0.2775		1Ti5	0.2761
	1Ti3	0.3029		2M1	0.2801		1Ti2	0.2885
Ti2−	2M3	0.2885		1Ti1	0.2891		1Ti3	0.2903
CN = 16	2M2	0.2893		2Ti4	0.3098		1Ti4	0.2916
	2M3	0.2921		2Ti4	0.3125		1Ti2	0.2921
	2Ti4	0.2944		1Ti2	0.3146		1Ti1	0.2935
	2M5	0.2953		1Ti2	0.3223	M4−	4M3	0.2489
	2M4	0.2971	M1−	2M2	0.2487	CN = 12	2M5	0.2571
	1Ti3	0.3088	CN = 12	2M3	0.2537		2Ti4	0.2805
	1Ti5	0.3146		1M6	0.2546		4Ti2	0.2971
	1Ti2	0.3215		2Ti5	0.2801	M5−	2M2	0.2462
	1Ti5	0.3223		1Ti4	0.2850	CN = 12	1M6	0.2534
Ti3−	1M5	0.2884		1Ti1	0.2871		1M4	0.2571
CN = 16	1M6	0.2891		1Ti4	0.2878		2M3	0.2574
	2M3	0.2903		2Ti1	0.2980		1Ti4	0.2806
	2M5	0.2922	M2−	1M2	0.2445		1Ti3	0.2884
	2M6	0.2929	CN = 12	1M5	0.2462		2Ti3	0.2922
	2M2	0.2929		1M6	0.2478		2Ti2	0.2953
	2M2	0.2973		1M1	0.2487	M6−	2M2	0.2478
	1Ti1	0.3029		1M2	0.2552	CN = 12	1M5	0.2534
	2Ti3	0.3051		1Ti5	0.2775		1M1	0.2546
	1Ti2	0.3088		1Ti2	0.2893		2M3	0.2575
Ti4−	1Ti4	0.2746		1Ti1	0.2915		1Ti3	0.2891
CN = 15	1M4	0.2805		1M5	0.2922		1Ti1	0.2902
	1M5	0.2806		1Ti3	0.2929		2Ti1	0.2915
	1M1	0.2850		1Ti3	0.2973		2Ti3	0.2929
	1M1	0.2878						

Table 3. Observed Scattering Power and Collected Occupancies for Different Models of Site Preference in τ_6

			calculated occupancy													
			Ti + Ni + Al			Ti + Ni				Ti + Al				Ni + Al			
	observed scattering power		X-rays + neutrons			X-rays		neutrons		X-rays		neutrons		X-rays		neutrons	
site	neutrons	X-rays	Ti	Ni	Al	Ti	Ni	Ti	Ni	Ti	Al	Ti	Al	Ni	Al	Ni	Al
M1	0.574	19.88	0.08	0.41	0.51	1.35	−0.35	0.33	0.67	0.76	0.24	−0.33	1.33	0.46	0.54	0.33	0.67
M2	0.595	20.44	0.08	0.45	0.47	1.26	−0.26	0.32	0.68	0.83	0.17	−0.36	1.36	0.50	0.50	0.37	0.63
M3	0.545	21.56	0.17	0.47	0.36	1.07	−0.07	0.35	0.65	0.95	0.05	−0.29	1.29	0.57	0.43	0.29	0.71
M4	0.403	21.56	0.31	0.39	0.31	1.07	−0.07	0.46	0.54	0.95	0.05	−0.08	1.08	0.57	0.43	0.08	0.92
M5	0.573	21.56	0.15	0.48	0.37	1.07	−0.07	0.33	0.67	0.95	0.05	−0.33	1.33	0.57	0.43	0.33	0.67
M6	0.375	17.92	0.18	0.22	0.60	1.68	−0.68	0.48	0.52	0.55	0.45	−0.04	1.04	0.33	0.67	0.04	0.96

atom positions and particularly to check on the electron density at the centers of vacant metal octahedra.

2. EXPERIMENTAL DETAILS

In order to find the reaction types and reaction temperatures related to τ_6, we have prepared 60 alloys (each of 1−2 g) from high purity metal ingots of Ti, Ni, and Al (purity 99.9 mass %, Alfa Johnson Matthey GmbH, D) by arc melting under argon atmosphere. Alloys were melted three times for homogenization (weight loss less than 0.1%). Then, the reguli were wrapped in Mo-foil to protect them from attack by the hot quartz walls, sealed in evacuated quartz tubes, and annealed for 10 days at temperatures from 850 to 1000 °C in steps of 5−10°. Temperature at the position of samples was controlled by a high quality standard thermocouple: the melting points of metal standards (5N-Ag, 5N-Cu) in the furnace used for all our annealing procedures were recorded within ±3 °C of the temperature listed in the International Temperature Scale ITS-90. All samples were quenched in cold water after annealing. Lattice parameters and standard deviations were determined by least-squares refinements of room temperature X-ray powder diffraction (XRD) data recorded with a Guinier-Huber image plate employing monochromatic Cu $K\alpha_1$ radiation. As-cast and annealed samples were polished using standard procedures and were examined by optical metallography and scanning electron microscopy (SEM). Compositions

dx.doi.org/10.1021/ic200245m |Inorg. Chem. 2011, 50, 4537–4547

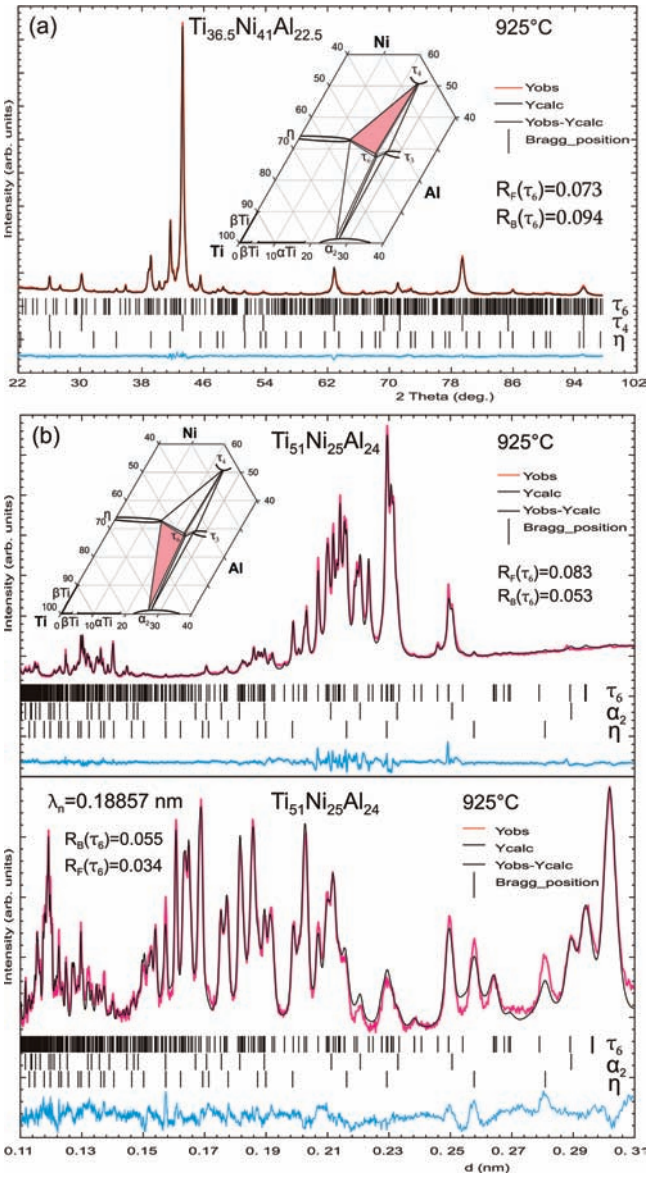

Figure 1. Rietveld refinements on room temperature spectra (a) for $Ti_{36.5}Ni_{41}Al_{22.5}$ (annealed and quenched from 925 °C) showing the three-phase equilibrium $\tau_6 + \tau_4 + \eta$ and (b) for $Ti_{51}Ni_{25}Al_{24}$ (annealed and quenched from 925 °C) revealing the three-phase equilibrium $\tau_6 + \alpha_2 + \eta$. Part b shows the pattern resulting from the combined refinement of XRD and NPD presented as intensities versus d values for both spectra. Vertical bars represent location of indexed peaks.

were determined in an electron probe microanalyzer (EPMA) on a Carl Zeiss EVO 40 equipped with a Pentafet Link EDX system operated at 20 kV. Pure elements were used as standards to carry out the deconvolution of overlapping peaks and background subtraction. Finally, the X-ray intensities were corrected for ZAF effects using the INCA-Energy 300 software package.[19] Overall composition of the samples derived from EPMA area scans agree with the nominal values within 0.5 at. %.

Thermal analyses were performed in a calibrated Netzsch STA 409 PG/4/G Luxx differential scanning calorimeter (DSC) employing a heating rate of 1−5 K/min in Al_2O_3 crucibles under a stream of 6N argon. Prior to DTA (differential thermal analysis), the alloys were annealed at 850 °C for 10 days.

Single crystals of τ_6 ($30 \times 35 \times 35$ nm^3) as well as of η-$(Ti,Al)_2Ni$ ($60 \times 50 \times 50$ nm^3) were mechanically isolated from arc-melted

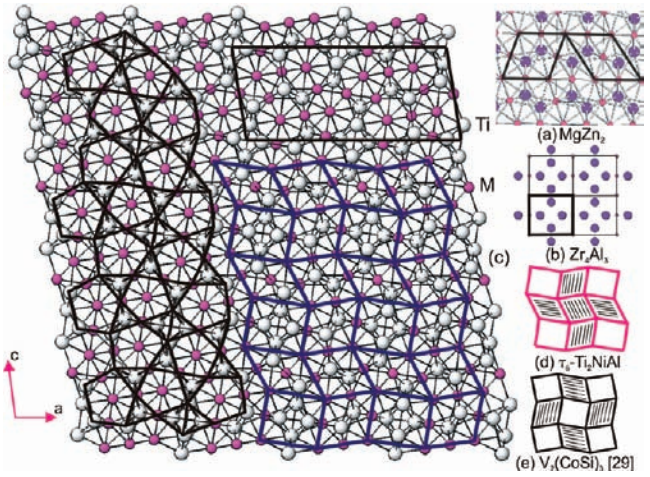

Figure 2. Crystal structure of $Ti_2(Ti_{0.16}Ni_{0.43}Al_{0.41})_3$ as seen in projection along the [010] axis: (a) thick lines highlighting the building blocks of $MgZn_2$, (b) Zr_4Al_3-unit highlighted with thick lines, (c) unit cell of $Ti_2(Ti_{0.16}Ni_{0.43}Al_{0.41})_3$ shown in upper right part, with left part indicating the pentagon−triangle main layers and right part showing blocks of $MgZn_2$ and Zr_4Al_3 forming the structure of τ_6, and (d) schematic arrangement of $MgZn_2$ (hexagonal ruled boxes) and Zr_4Al_3 units (square unruled boxes) according to this work outlined in contrast to (e) the version shown for $V_2(Co_{0.57}Si_{0.43})_3$ in Typix.[29].

specimens $Ti_{54}Ni_{25}Al_{21}$ and $Ti_{54.3}Ni_{32.3}Al_{13.4}$, which were annealed at 975 and 980 °C, respectively. The crystals were inspected on an AXS-GADDS texture goniometer for quality and crystal symmetry prior to X-ray intensity data collection on a four-circle Nonius Kappa diffractometer (CCD area detector and graphite monochromated Mo K_α radiation, λ = 0.071 069 nm). Orientation matrix and unit cell parameters were derived using the program DENZO.[20] No absorption correction was necessary because of the rather regular crystal shape and small dimensions of the investigated specimens. The structures were solved by direct methods and refined with the SHELXS-97 and SHELXL-97 programs,[21] respectively.

As for neutron powder diffraction (NPD), a sample with a total mass of about 6 g was necessary; 10 individual alloys of smaller mass (1 g) to facilitate quenching were prepared (at the nominal composition $Ti_{51}Ni_{25}Al_{24}$ and annealed at 925 °C), from which six specimens with identical lattice parameters for the τ_6-phase were selected and powdered to a grain size below 40 μm in order to reduce preferential orientation effects. Neutron diffraction was performed at room temperature on the high resolution HRPT diffractometer[22] at the SINQ spallation source of the Paul Scherrer Institute (Switzerland). The diffractometer was used in high intensity mode ($\Delta d/d \geq 2 \times 10^{-3}$) with a neutron wavelength $\lambda_{neutron}$ = 0.188 570 nm within the angular 2θ range from 3.85° to 164.2°. Combined Rietveld multipattern refinements of the X-ray and neutron powder diffraction data were performed with the FULLPROF program[23] with the use of its internal tables for scattering lengths and atom form factors.

3. RESULTS AND DISCUSSION

3.1. Crystal Structure of τ_6-$Ti_2(Ti_{0.16}Ni_{0.43}Al_{0.41})_3$ from Combined X-ray Single Crystal and X-ray Powder and Neutron Powder Diffraction Analyses. Unit cell parameters [a = 1.85383(7) nm, b = 0.49970(2) nm, c = 0.81511(3) nm, β = 99.597(3)°] and systematic extinctions for a C-centered lattice are compatible with three monoclinic space group symmetries: $C2$, Cm, and $C2/m$. Solution of the structure by direct methods in all these space groups revealed the same atomic order in the crystal lattice. As practically identical reliability factors and

dx.doi.org/10.1021/ic200245m |Inorg. Chem. 2011, 50, 4537–4547

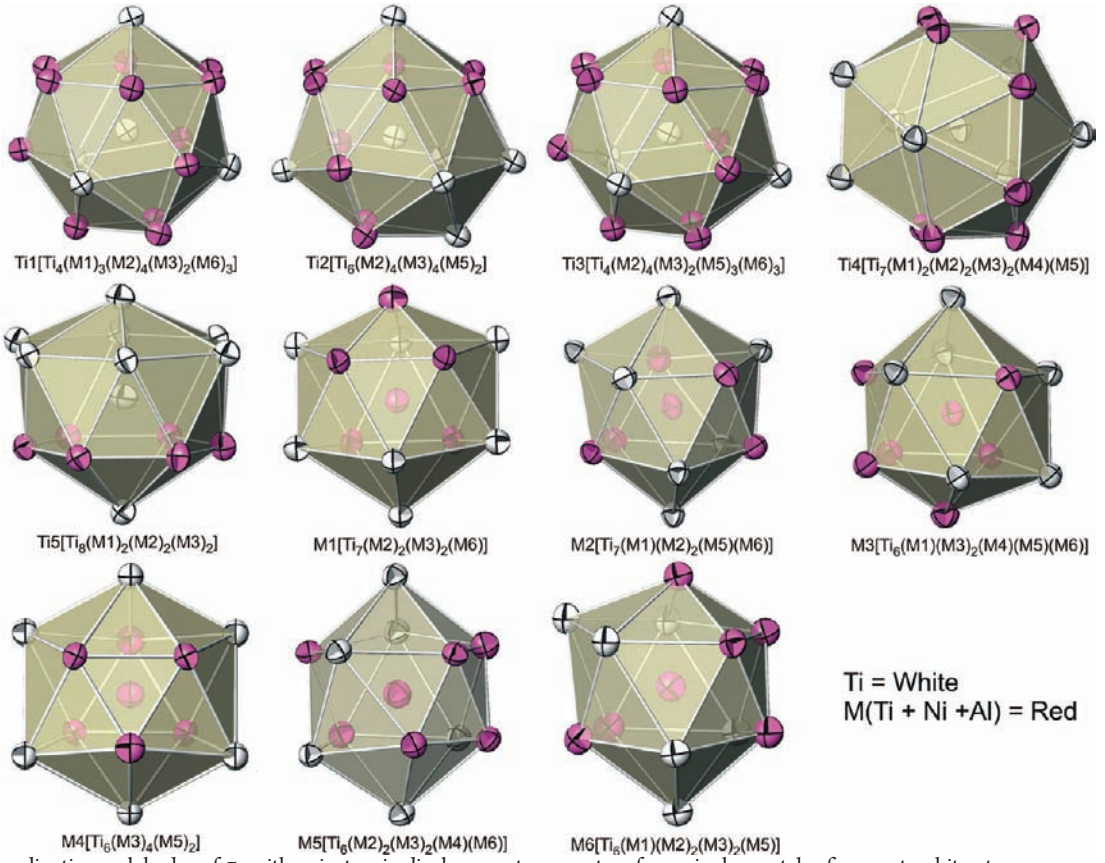

Figure 3. Coordination polyhedra of τ_6 with anisotropic displacement parameters from single crystal refinement: white atoms represent a position occupied by Ti atoms only, and red atoms (dark gray in black and white print) represent the mixed positions of Ti + Ni + Al.

Table 4. Architecture of Crystal Structures Derived from the $V_2(Co_{0.57}Si_{0.43})_3$-Type, All with Space Group C12/*m*1 (No. 12)

Compound	$Ti_2(Ti_{0.16}Ni_{0.43}Al_{0.41})_3$	$V_2(Co_{0.57}Si_{0.43})_3$	$Mg_{2.30}Ir_{2.70}$	$Mg_{1.93}Ir_{3.07}$
Reference	This work	[26]	[27]	[28]
composition from refinement	$Ti_2(Ti_{0.16}Ni_{0.43}Al_{0.41})_3$	$V_2(Co_{0.57}Si_{0.43})_3$	$Mg_2(Mg_{0.1}Ir_{0.9})_3$	$(Mg_{0.97}Ir_{0.03})_2Ir_3$
a (nm)	1.853 83(7)	1.717	1.8582(2)	1.856 99(2)
b (nm)	0.499 70(2)	0.466	0.523 08(6)	0.518 715(4)
c (nm)	0.815 11(3)	0.755	0.8551(1)	0.849 233(6)
β (°)	99.597(3)	99.2	97.645(9)	97.2209(5)
4i (*x*, 0, *z*)	**Ti**	**V**	**Mg**	**Mg**
x, *z*	0.285 39(4), 0.079 94(10)	0.294, 0.091	0.2803(3), 0.0851(8)	0.281(1), 0.067(2)
4i (*x*, 0, *z*)	**Ti**	**V**	**Mg**	**Mg**
x, *z*	0.551 66(4), 0.359 96(10)	0.553, 0.369	0.5543(3), 0.3831(7)	0.562(1), 0.382(2)
4i (*x*, 0, *z*)	**Ti**	**V**	**Mg**	**Mg**
x, *z*	0.289 16(4), 0.452 92(10)	0.294, 0.440	0.2913(3), 0.4474(7)	0.286(1), 0.435(2)
4i (*x*, 0, *z*)	**Ti**	**V**	**Mg**	**Mg**
x, *z*	0.023 60(4), 0.168 85(10)	0.015, 0.144	0.0227(3), 0.1803(7)	0.025(1), 0.174(2)
4i (*x*, 0, *z*)	**Ti**	**V**	**Mg**	0.167(5)Ir + 0.833Mg
x, *z*	0.434 72(4), 0.019 64(10)	0.427, 0.015	0.4218(3), 0.0093(7)	0.4228(5), 0.007(1)
4i (*x*, 0, *z*)	0.073(1) **Ti** + 0.462 **Ni** + 0.465 **Al**	0.57 **Co** + 0.43 **Si**	0.926(5) **Ir** + 0.074 **Mg**	**Ir**
x, *z*	0.868 94(4), 0.0437(1)	0.873, 0.037	0.871 63(3), 0.031 92(7)	**0.8702(2), 0.0294(3)**
8j (*x*, *y*, *z*)	0.136(1) **Ti** + 0.421 **Ni** + 0.443 **Al**	0.57 **Co** + 0.43 **Si**	**Ir**	**Ir**
x, *y*, *z*	0.1687(1), 0.2553(1), 0.2185(1)	0.164, 0.25, 0.225	0.166 41(2), 0.253 47(7), 0.226 35(5)	0.1676(1), 0.2496(4), 0.2271(2)
8j (*x*, *y*, *z*)	0.164(1) **Ti** + 0.507 **Ni** + 0.329 **Al**	0.57 **Co** + 0.43 **Si**	**Ir**	**Ir**
x, *y*, *z*	0.4076(1), 0.2358(1), 0.3097(1)	0.407, 0.25, 0.308	0.409 58(2), 0.233 69(7), 0.297 47(4)	0.4095(1), 0.2357(3), 0.2957(2)
2c (0, 0, $^1/_2$)	0.262(2) **Ti** + 0.440 **Ni** + 0.298 **Al**	0.57 **Co** + 0.43 **Si**	0.694(8) **Ir** + 0.306 **Mg**	**Ir**
4i (*x*, 0, *z*)	0.151(2) **Ti** + 0.488 **Ni**+ 0.361 **Al**	0.57 **Co** + 0.43 **Si**	0.836(6) **Ir** + 0.164 **Mg**	**Ir**
x, *z*	0.133 47(4), 0.451 01(10)	0.129, 0.464	0.13530(3), 0.46351(7)	0.1351(2), 0.4655(3)
4i (*x*, 0, *z*)	0.238(1) **Ti** + 0.237 **Ni** + 0.525 **Al**	0.57 **Co** + 0.43 **Si**	0.652(6) **Ir** + 0.348 **Mg**	**Ir**
x, *z*	0.213 34(5), 0.735 38(11)	0.206, 0.735	0.215 13(3), 0.7443(1)	**0.2144(2), 0.7408(3)**
R_F^2	0.0376	Not Given	0.0335	R_B = 0.056
Technique of measurement	XSC + NPD + XRD	XSC	XSC	XRD

dx.doi.org/10.1021/ic200245m |*Inorg. Chem.* 2011, 50, 4537–4547

Table 5. X-ray Single Crystal Data for η-$(Ti_{1-x}Al_x)_2Ni$[a]

parameter	$(Ti_{0.84}Al_{0.16})_2Ni$
composition from EPMA (at. %)	$Ti_{56.7}Ni_{32.3}Al_{11.0}$
composition from refinement (at. %)	$Ti_{55.7}Ni_{33.3}Al_{11.0}$
formula from refinement	$(Ti_{1-x}Al_x)_2Ni$; x = 0.16
a (nm)	1.125 43(3)
μ_{abs} (mm^{-1})	17.41
V (nm^3)	1.4255
ρ_x (g cm^{-3})	5.50
reflns in refinement	168 > 4$\sigma(F_o)$ of 196
mosaicity	0.55
no. of variables	15
$R_F^2 = \Sigma\|F_o^2 - F_c^2\|/\Sigma F_o^2$	0.0222
R_{Int}	0.060
wR2	0.050
GOF	1.151
extinction (Zachariasen)	0.00026(7)
residual density $e^-/Å^3$, max; min	1.49; −0.68
atom parameters	
Ni1 in 32e (x, x, x); x; occ	1.00Ni; x = 0.213 69(3)
$U_{11} = U_{22} = U_{33}$	0.0106(2)
$U_{23} = U_{13} = U_{12}$	0.0010(1)
M1 (Ti1/Al1) in 48f (x, $^1/_8$, $^1/_8$); x	0.800(4)Ti + 0.200Al; x = 0.440 13(6)
U_{11}; $U_{22} = U_{33}$	0.0101(3); 0.0088(2)
U_{23}, $U_{13} = U_{12}$	0.0006(2), 0.0000
M2 (Ti2/Al2) in 16c (0, 0, 0) occ	0.944(4)Ti + 0.056Al
$U_{11} = U_{22} = U_{33}$	0.0101(2)
$U_{23} = U_{13} = U_{12}$	0.0016(2)

[a] x = 0.16. Space group $Fd\bar{3}m$, No. 227 (Ti_2Ni structure type) standardized with program *Structure Tidy*.[24] Data collection details: Mo Kα; 2° ≤ 2Θ ≤ 72.05°; ω-scans, scan width 2°; 150 s/frame.

residual electron densities were obtained for these three refinements and as an analysis of missing symmetry by program PLATON confirmed 2/m, we describe the structure in the highest symmetric space group $C2/m$. Including anisotropic atomic displacement parameters for all atoms, the refinement converged to R_{F2} = 0.038 with residual electron densities ≤1.4 $e^-/10^{-3}$ nm^3. At this stage, the composition of τ_6, as derived from the single crystal refinement, was $Ti_{53.22}Ni_{25.26}Al_{21.22}$, close to the formula "$Ti_2NiAl$" and within 2 −3 atom % of the EPMA data. Although XRD intensities collected from a polycrystalline sample are in perfect agreement with the intensities calculated from the structural model taken from the single crystal, a corresponding neutron powder spectrum showed severe discrepancies and was not explained to satisfaction. Due to the negative neutron scattering length of natural titanium, neutron powder diffraction data are very sensitive to the location of Ti atoms in the lattice, whereas the occupation of a random mixture of Ni and Al atoms in proper proportions may constitute the X-ray scattering power of a titanium atom (at $(\sin\theta)/\lambda = 0$: $0.60 \times f_{Ni} + 0.40 \times f_{Al} = f_{Ti}$). Therefore, a combined analysis of XRD and NPD data is necessary to unambiguously define the site preference. Although refinement of the neutron powder data unambiguously confirmed the five crystallographic positions (Ti1−Ti5, see Tables 1 and 2) completely occupied by Ti, refinements of random mixtures of two atom species for the remaining six crystallographic sites were unsuccessful.

Again atom ordering in lower symmetry (space group types Cm and $C2$) was pursued to no avail. Therefore, we returned to the higher symmetry $C2/m$, and in order to define the combination of atoms per site (keeping the five Ti-sites already determined), we simply refined the electron density and the nucleon density on every site M1 to M6 (Table 3). This procedure yields for each site a system

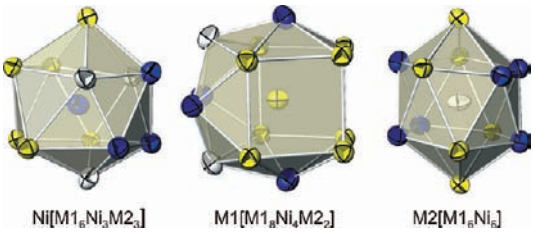

Figure 4. Coordination polyhedra of the atom sites in η-$(Ti_{0.84}Al_{0.16})_2Ni$ with anisotropic displacement parameters from single crystal refinement. Blue atoms (dark gray in black and white print) represent a position occupied by Ni atoms only, yellow atoms (light gray in black and white print) represent the mixed position M1 (0.80Ti + 0.20Al), and white atoms represent the mixed position M2 (0.94Ti + 0.06Al).

Table 6. Interatomic Distances (nm) for τ_6 Taken from XSC Refinement (Upper Right Column), Standard Deviation ≤ 0.0001 nm

Ni1−	3M2	0.2473	M1−	2Ni1	0.2581		4M1	0.2998
CN = 12	3M1	0.2581	CN = 14	2Ni1	0.2913	M2−	6Ni1	0.2473
	3Ni1	0.2823		2M2	0.2922	CN = 12	6M1	0.2922
	3M1	0.2913		4M1	0.2943			

of two equations with two variables, the solution of which presents the corresponding random mixture of atoms for each site. The calculations, which are summarized in Table 3, unambiguously imply a mix of the three atom species Ti, Ni, Al on all these sites. A combined XRD and NPD refinement of this model was satisfactory (see Figure 1, Table 3): (1) it confirmed the atom arrangement derived from the calculation, and (2) without using the phase composition as a constraint, the proper atom concentrations were obtained. It should be emphasized that crystallographic models that involve a random mixture of only two atom species in sites M1−M6 (Ti + Ni or Ti + Al; for details see Table 3) result in negative occupancies. Even for M1 and M2 sites, for which the calculation yielded a minor amount of Ti as a third element, a random mix of three atom species is clearly required in order to achieve a proper ADP (atomic displacement parameter). On the basis of this atom distribution, the refinement of the X-ray single crystal data gained only marginal improvement with R_{F2} = 0.037 and residual electron densities ≤1.4 $e^-/10^{-3}$ nm^3. However, as a final composition from the refinement, we arrive at τ_6-$Ti_2(Ti_{0.16}Ni_{0.43}Al_{0.41})_3$, now within 1 atom % of the EPMA data (Tables 1 and 2).

A search for the structure type (Pearson symbol: mS50) in *Pearson's Crystal Data*[25] prompted two compounds, which adopt the same crystal symmetry and Wyckoff sequence, i.e., the structures of $V_2(Co_{0.57}Si_{0.43})_3$[26] and $Mg_{2.3}Ir_{2.7}$.[27] A comparison of the atom site occupation in τ_6 with these structures is consistent with the fact that the larger polyhedral centers (CN = 14, 15, and 16; distorted Franck−Kasper polyhedra) are occupied by the larger and more electropositive elements V, Mg, and Ti.

The crystal structure of τ_6-$Ti_2(Ti_{0.16}Ni_{0.43}Al_{0.41})_3$ is presented in Figure 2 as seen along the [010] axis and clearly shows the pentagon−triangle main layers of metal atoms. Krypyakevich[26] recognized units of $MgZn_2$ and Zr_4Al_3 (shown in the lower left part of Figure.2) as the building blocks of $V_2(Co_{0.57}Si_{0.43})_3$. The arrangement of these building blocks of corresponding units of $MgZn_2$ (τ_3 in the Ti−Ni−Al system) and Zr_4Al_3 is outlined by thick solid lines in the right part of the crystal structure of τ_6 in Figure 2. A comparison of the schematic arrangement of $MgZn_2$

dx.doi.org/10.1021/ic200245m |*Inorg. Chem.* 2011, 50, 4537–4547

Table 7. Composition (EPMA) and Lattice Parameters for Selected Alloys

	Nominal (at. %)			Overall (at. %)						Cell parameters (nm)			Composition (at. %)		
no.	Ti	Ni	Al	Ti	Ni	Al	H. T.* (°C)	Phases	S. G., Str. Type	*a*	*b*	*c*	Ti	Ni	Al
1	44	33	23	42.3	33.4	24.3	1000	τ_3	$P6_3/mmc$, $MgZn_2$	0.501 27(3)		0.806 75(8)	47.5	28.4	24.1
								η	$Fd\bar{3}m$, Ti_2Ni	1.123 48(5)			54.1	30.4	15.5
								τ_4	$Fm\bar{3}m$, $MnCu_2Al$	0.590 32(8)			27.0	49.0	24.0
2	51	25	24	49.1	25.4	25.5	1000	α_2	$P6_3/mmc$, Mg_3Cd	0.579 46(7)		0.466 86(0)	75.0	0.9	24.1
								τ_3	$P6_3/mmc$, $MgZn_2$	0.501 61(6)		0.807 53(9)	47.5	27.8	24.7
								η	$Fd\bar{3}m$, Ti_2Ni	1.123 62(4)			54.4	30.1	15.5
3	49.5	26	24.5	50.2	25.7	24.1	975	α_2	$P6_3/mmc$, Mg_3Cd	0.579 12(5)		0.465 23(6)	73.3	1.1	25.6
								τ_3	$P6_3/mmc$, $MgZn_2$	0.501 68(9)		0.809 05(9)	46.6	28.6	24.8
								τ_6	$C2/m$, $V_2(Co,Si)_3$	1.848 01(5)	0.498 99(1)	0.814 68(2)	49.5	27.1	23.4
4	50	28	22	51.1	28.1	20.8	975	η	$Fd\bar{3}m$, Ti_2Ni	1.123 67(3)			54.2	30.8	15.0
								τ_6	$C2/m$, $V_2(Co,Si)_3$	1.849 21(8)	0.499 03(2)	0.815 04(3)	49.6	27.1	23.3
								τ_3	$P6_3/mmc$, $MgZn_2$	0.501 48(4)		0.807 90(8)	46.7	29.0	24.3
5	51	25	24	50.8	25.5	23.7	975	α_2	$P6_3/mmc$, Mg_3Cd	0.579 22(4)		0.466 42(4)	73.8	1.0	25.2
								η	$Fd\bar{3}m$, Ti_2Ni	1.124 14(4)			54.8	30.1	15.1
								τ_6	$C2/m$, $V_2(Co,Si)_3$	1.847 77(5)	0.499 17(1)	0.814 15(2)	50.0	26.4	23.6
6	47	30	23	47.6	37.1	22.3	975	τ_3	$P6_3/mmc$, $MgZn_2$	0.501 41(4)		0.807 45(7)	46.4	29.0	24.6
								η	$Fd\bar{3}m$, Ti_2Ni	1.123 80(3)			54.0	31.6	14.4
								τ_4	$Fm\bar{3}m$, $MnCu_2Al$	0.589 67(20)			27.0	49.0	24.0
7	50	28	22	51.5	27.5	21.0	950	η	$Fd\bar{3}m$, Ti_2Ni	1.123 33(9)			53.8	32.1	14.1
								τ_6	$C2/m$, $V_2(Co,Si)_3$	1.848 35(6)	0.499 02(1)	0.813 84(3)	49.3	27.7	23.0
								τ_3	$P6_3/mmc$, $MgZn_2$	0.501 39(6)		0.808 39(7)	46.9	28.7	24.4
8	51	25	24	52.1	25.1	22.8	950	α_2	$P6_3/mmc$, Mg_3Cd	0.578 79(9)		0.465 51(8)	72.8	1.1	26.1
								η	$Fd\bar{3}m$, Ti_2Ni	1.123 83(9)			53.8	31.6	14.6
								τ_6	$C2/m$, $V_2(Co,Si)_3$	1.847 41(3)	0.498 87(1)	0.813 87(1)	49.2	26.6	24.2
9	49.5	26	24.5	50.2	25.7	24.1	950	α_2	$P6_3/mmc$, Mg_3Cd	0.578 55(5)		0.464 99(8)	72.6	1.1	26.3
								τ_3	$P6_3/mmc$, $MgZn_2$	0.501 54(7)		0.808 48(9)	46.2	28.6	25.2
								τ_6	$C2/m$, $V_2(Co,Si)_3$	1.848 21(5)	0.498 92(1)	0.814 40(2)	49.2	26.9	23.9
10	47	30	23	47.8	30.5	21.7	950	τ_3	$P6_3/mmc$, $MgZn_2$	0.501 28(3)		0.807 79(8)	46.4	28.7	24.9
								η	$Fd\bar{3}m$, Ti_2Ni	1.123 00(7)			54.2	31.7	14.1
								τ_4	$Fm\bar{3}m$, $MnCu_2Al$	0.589 90(4)			27.0	49.0	24.0
11	51	25	24	52.3	24.2	23.5	925	α_2	$P6_3/mmc$, Mg_3Cd	0.578 60(5)		0.465 09(8)	72.4	1.1	26.5
								η	$Fd\bar{3}m$, Ti_2Ni	1.123 10(9)			53.3	32.2	14.5
								τ_6	$C2/m$, $V_2(Co,Si)_3$	1.846 18(3)	0.498 93(1)	0.813 85(1)	48.6	27.3	24.1
12	36.5	41	22.5	38.1	39.9	21.9	925	τ_4	$Fm\bar{3}m$, $MnCu_2Al$	0.590 14(5)			26.6	49.5	23.9
								η	$Fd\bar{3}m$, Ti_2Ni	1.123 36(9)			52.8	33.2	14.0
								τ_6	$C2/m$, $V_2(Co,Si)_3$	1.847 16(9)	0.499 16(3)	0.814 24(4)	48.5	28.2	23.3
13	49	25	26	50.4	24.4	25.2	925	α_2	$P6_3/mmc$, Mg_3Cd	0.578 82(3)		0.465 44(9)	72.3	1.0	26.7
								τ_3	$P6_3/mmc$, $MgZn_2$	0.501 32(4)		0.808 62(7)	45.1	28.6	26.3
								τ_6	$C2/m$, $V_2(Co,Si)_3$	1.846 53(9)	0.499 14(3)	0.815 09(4)	48.3	27.0	24.7
14	44	30	26	45.4	29.3	25.3	925	τ_3	$P6_3/mmc$, $MgZn_2$	0.501 35(5)		0.808 29(8)	45.1	28.6	26.3
								τ_4	$Fm\bar{3}m$, $MnCu_2Al$	0.589 97(8)			26.8	49.0	24.2
								α_2	$P6_3/mmc$, Mg_3Cd	0.578 91(5)		0.465 97(9)	71.7	1.4	26.9
								η	$Fd\bar{3}m$, Ti_2Ni	1.123 21(9)			51.6	32.3	16.1
15	51	25	24	52.3	24.2	23.5	900	α_2	$P6_3/mmc$, Mg_3Cd	0.578 95(4)		0.465 31(6)	72.1	1.0	26.9
								η	$Fd\bar{3}m$, Ti_2Ni	1.123 68(9)			53.3	32.8	13.9
								τ_6	$C2/m$, $V_2(Co,Si)_3$	1.846 04(3)	0.498 67(1)	0.813 29(1)	48.1	27.9	24.0
16	48	25	27	49.1	24.5	26.4	900	α_2	$P6_3/mmc$, Mg_3Cd	0.578 81(7)		0.465 10(6)	71.9	1.0	27.1
								τ_4	$Fm\bar{3}m$, $MnCu_2Al$	0.589 82(9)			26.4	49.0	24.6
								τ_3	$P6_3/mmc$, $MgZn_2$	0.501 16(6)		0.807 57(7)	44.3	28.7	27.0
17	36.5	41	22.5	38.5	39.9	21.6	900	τ_4	$Fm\bar{3}m$, $MnCu_2Al$	0.589 95(8)			25.4	50.6	24.0
								η	$Fd\bar{3}m$, Ti_2Ni	1.123 32(9)			52.4	33.8	13.8
								τ_6	$C2/m$, $V_2(Co,Si)_3$	1.846 84(9)	0.499 76(5)	0.814 03(8)	48.1	28.0	23.9
18	49.5	26	24.5	51.0	25.1	23.9	900	α_2	$P6_3/mmc$, Mg_3Cd	0.578 65(6)		0.465 10(8)	71.9	1.1	27.0
								τ_4	$Fm\bar{3}m$, $MnCu_2Al$	0.589 58(8)			26.0	50.0	24.0
								τ_6	$C2/m$, $V_2(Co,Si)_3$	1.845 79(4)	0.498 59(1)	0.813 06(2)	48.3	27.7	24.0
19	46	27	27	47.9	25.6	26.5	865	α_2	$P6_3/mmc$, Mg_3Cd	0.578 65(7)		0.464 07(5)	71.7	1.0	27.3
								τ_4	$P6_3/mmc$, $MgZn_2$	0.590 21(1)			25.3	50.6	24.1
								τ_3	$P6_3/mmc$, $MgZn_2$	0.501 61(5)		0.807 54(7)	42.1	29.0	28.9
20	47	31	22	48.7	29.5	21.8	865	α_2	$P6_3/mmc$, Mg_3Cd	0.579 35(8)		0.463 89(5)	72.3	1.0	26.7
								τ_4	$Fm\bar{3}m$, $MnCu_2Al$	0.590 06(7)			25.4	51.0	23.6
								η	$Fd\bar{3}m$, Ti_2Ni	1.123 55(9)			52.8	34.2	13.0

and Zr_4Al_3 units according to this work with the version given in Typix for $V_2(Co_{0.57}Si_{0.43})_3$[29] is outlined in the upper left part of Figure 2 and questions the correctness of the stacking sequence presented earlier.[29]

dx.doi.org/10.1021/ic200245m |*Inorg. Chem.* 2011, 50, 4537–4547

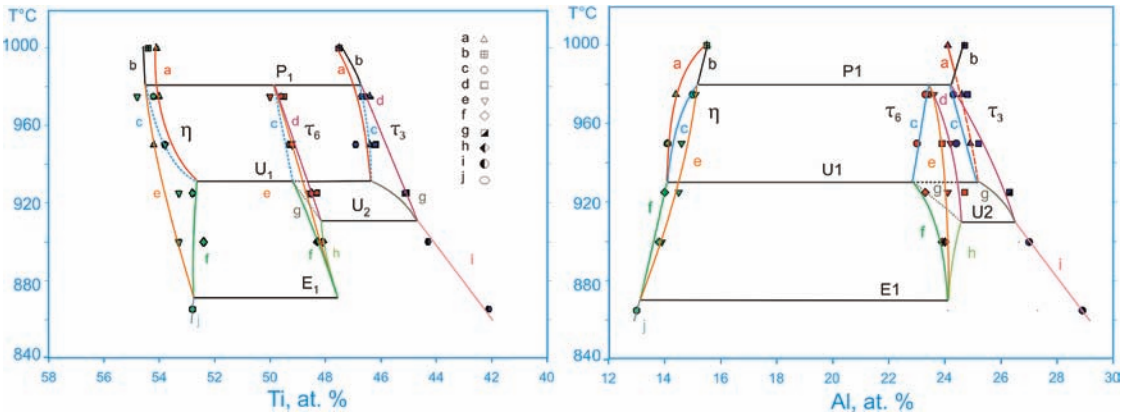

Figure 5. Temperature dependence of vertex-composition of η, τ_3, τ_6; line a represents triangle $\eta + \tau_3 + \tau_4$, b represents triangle $\eta + \alpha_2 + \tau_3$, c represents triangle $\eta + \tau_3 + \tau_6$, d represents triangle $\alpha_2 + \tau_3 + \tau_6$, e represents triangle $\eta + \alpha_2 + \tau_6$, f represents triangle $\eta + \tau_4 + \tau_6$, g represents triangle $\tau_3 + \tau_4 + \tau_6$, h represents triangle $\alpha_2 + \tau_4 + \tau_6$, i represents triangle $\alpha_2 + \tau_3 + \tau_4$, and j represents triangle $\eta + \alpha_2 + \tau_4$.

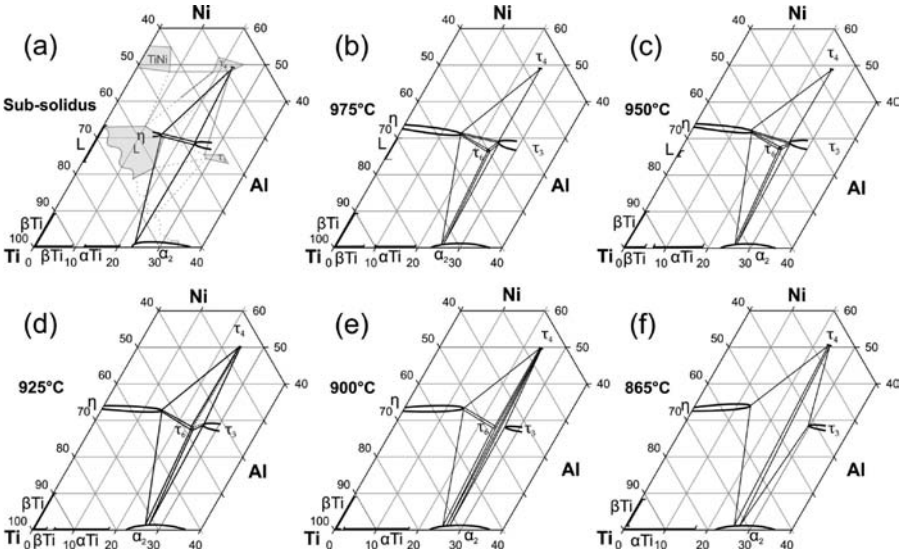

Figure 6. Partial phase diagrams at (a) subsolidus (slightly below solidus) temperature, (b) 975 °C, (c) 950 °C, (d) 925 °C, (e) 900 °C, and (f) 865 °C. Equilibria at 1000° after ref 10 are shown in gray (a).

A listing of the interatomic distances in $Ti_2(Ti_{0.16}Ni_{0.43}Al_{0.41})_3$ is presented in Table 2. The bonds between Ti−Ti, Ti−M, and M−M are in the ranges 0.249−0.322, 0.276−0.301, and 0.236−0.264 nm, respectively. Shortest interatomic distances are associated with M sites containing higher Ni content. Due to the lack of precise atom positions for $V_2(Co_{0.57}Si_{0.43})_3$,[26] no comparison can be made. The coordination polyhedra for all independent crystal sites in τ_6 are presented in Figure 3.

From the comparison of the atom site occupation in τ_6 with the isopointal structures of $V_2(Co_{0.57}Si_{0.43})_3$[26] and $Mg_{2.3}Ir_{2.7}$[27] in Table 4, we conclude that the larger polyhedral centers (CN = 14, 15, and 16; distorted Franck−Kasper polyhedra) are occupied by the larger and more electropositive elements V, Mg, and Ti, while all the smaller M atom combinations are found at the centers of distorted icosahedra. Atoms Ti1, Ti2, and Ti3 in τ_6 adopt the same polyhedra like Mg in $MgZn_2$; M7, M8, and M11 correspond to polyhedra of Zn2 in $MgZn_2$; but M1 and M2 were found to be surrounded by identical polyhedra like Al in Zr_4Al_3.

3.2. Crystal Structure of η-$(Ti_{0.84}Al_{0.16})_2Ni$. A single crystal was selected from the alloy $Ti_{55.7}Ni_{33.1}Al_{11.2}$ (composition from EPMA) annealed at 980 °C to derive high precision atom positions and particularly to check on the electron density at the centers of vacant metal octahedra. X-ray single crystal data were completely indexed on a cubic face centered lattice, and extinctions $(0kl)$ for $k + l = 4n + 1$, and $(h00)$ for $h = 4n + 1$, confirm $Fd\bar{3}m$ as the space group with the highest symmetry. Direct methods confirm atom order isotypic with the Ti_2Ni-type. For anisotropic atomic displacement parameters, the refinement converged to $R_{F2} = 0.023$ with residual electron densities smaller than 1.5 $e^-/10^{-3}$ nm^3. Results are compiled in Tables 5 and 6. In agreement with the extension of the solid solution η-$(Ti_{1-x}Al_x)_2Ni$, Al atoms at $x = 0.16$ substitute for 20% of the Ti atoms in the 48f position $(x, {}^1/_8, {}^1/_8)$, whereas Al atoms in the 16c position $(0, 0, 0)$ at the centers of metal icosahedra substitute for 5.6% of the Ti atoms. Ni-atoms occupy the 32e site (x, x, x). It should be noted that residual densities (1.5 $e^-/10^{-3}nm^3$) are insignificant and demonstrate that there is a negligible concentration of nonmetal

dx.doi.org/10.1021/ic200245m |Inorg. Chem. 2011, 50, 4537–4547

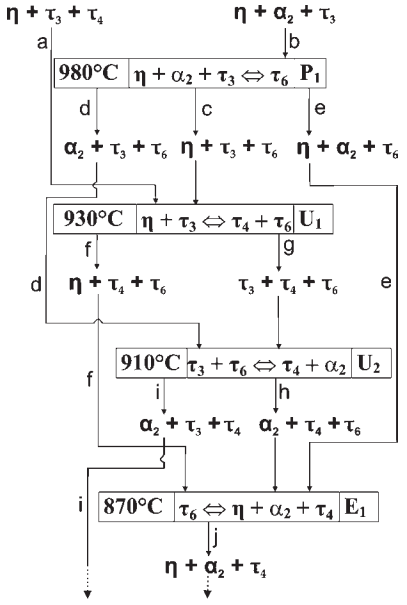

Figure 7. Schultz–Scheil diagram involving the phase τ_6-$Ti_2(Ti_{0.16}Ni_{0.43}Al_{0.41})_3$. Letters a, b, and so forth correspond to three-phase triangles for which composition dependence as a function of temperature is shown in Figure 5.

atoms at the centers of Ti/Al octahedra (16d sites ($^1/_2$, $^1/_2$, $^1/_2$) and 8b sites ($^3/_8$, $^3/_8$, $^3/_8$)). Thus, stabilization of the solid solution η-$(Ti_{1-x}Al_x)_2$-Ni by interstitials can safely be ruled out. The composition obtained from the structure refinement, $Ti_{56.7}Ni_{32.3}Al_{11}$, is almost identical with the EPMA value (see Table 5).

The coordination polyhedra for η-$(Ti_{0.84}Al_{0.16})_2Ni$ are shown in Figure 4. Interatomic distances are listed in Table 6. The shortest bond distances are observed between Ni1 and Ti4, whereas longest distances are observed between Ti2 and Al3 or Ti2 with Ti2 itself. Ti–Ni, Ti–Al, and Ni–Al bonds are found to be in the ranges 0.247–0.291, 0.292–0.294, and 0.258 nm, respectively. A comparison of interatomic distances of η-$(Ti_{0.84}Al_{0.16})_2Ni$ with binary Ti_2Ni shows that our bond distances, $d_{Ni\text{-}M}$ = 0.2473–0.2913 nm, d_{Ni-Ni} = 0.2823 nm, and $d_{M\text{-}M}$ = 0.2922–0.2998 nm, are in good agreement with data in the literature.[25,29] It should be noted that although Ti sites are partially occupied by Al atoms, still the bond distance remains the same because of the similar size of Ti and Al atoms.

3.3. Phase Equilibria and Reactions Involving the τ_6-Phase. In our previous investigation,[7] the Laves phase (τ_3) was found to form equilibrium with α_2-Ti_3Al and τ_4-$TiNi_2Al$ at 900 °C, while alloys annealed at 1000 °C contained the Laves phase together with the liquid. At temperatures between 980 and 870 °C, a new X-ray powder diffractogram was recognized suggesting the formation of a novel ternary compound for which X-ray and EPMA data revealed a formula "Ti_2NiAl". XRD spectra are consistent with the spectra collected by Grytsiv et al.[17] on a new phase near "Ti_2NiAl" ($Ti_{47-49}Ni_{27}Al_{26-24}$). Rietveld refinement of the XRD intensities undoubtedly identified the spectra with the crystal structure of τ_6-$Ti_2(Ti_{0.16}Ni_{0.43}Al_{0.41})_3$. According to EPMA, a small homogeneity region (~1 at. %) (Table 7, Figure 5) was found.

Figure 5 presents the temperature dependence of the composition of the phases involved in equilibria with the τ_6-phase. The corresponding change in lattice parameters is in most cases small

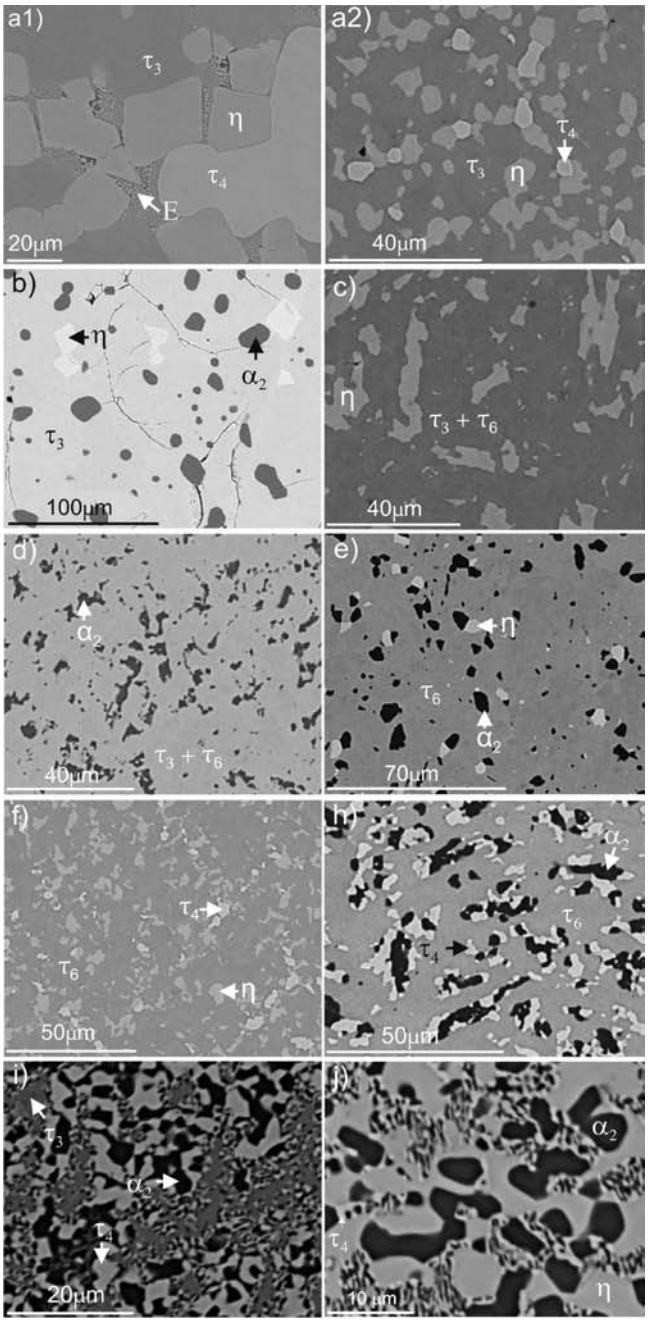

Figure 8. Microstructures of selected samples with phases identified by EPMA: (a1) $Ti_{47}Ni_{30}Al_{23}$ (1000 °C), (a2) $Ti_{47}Ni_{30}Al_{23}$ (950 °C), (b) $Ti_{51}Ni_{25}Al_{24}$ (1000 °C), (c) $Ti_{50}Ni_{28}Al_{22}$ (975 °C), (d) $Ti_{49}Ni_{25}Al_{26}$ (975 °C), (e) $Ti_{51}Ni_{25}Al_{24}$ (975 °C), (f) $Ti_{48}Ni_{29}Al_{23}$ (925 °C), (h) $Ti_{49.5}Ni_{26}Al_{24.5}$ (900 °C), (i) $Ti_{46}Ni_{27}Al_{27}$ (865 °C), (j) $Ti_{56}Ni_{25.0}Al_{19}$ (865 °C). Phase compositions and lattice parameters are available in Table 7.

as the phases mainly shift their composition with respect to Ti/Al substitution with similar atom radii for Ti and Al.

X-ray and EPMA results of selected samples to prove isothermal equilibria at various temperatures are summarized in Table 7. Due to slow reaction kinetics, even at very slow heating rates (1 K/min), it was very difficult to interpret DSC measurements. Therefore, X-ray and EPMA on isothermally treated alloys served to construct isothermal phase relations for the region confined by the phases $TiNi_2Al$ (τ_4), $(Ti_{1-x}Al_x)_2Ni$ (η),

dx.doi.org/10.1021/ic200245m |Inorg. Chem. 2011, 50, 4537–4547

Table 8. Invariant Equilibria Involving τ_6

Invariant Equilibrium	phase	composition (at. %)		
		Ti	Ni	Al
P_1: 980 °C	α_2	73.6	~1.0[a]	25.4
$\eta + \alpha_2 + \tau_3 \leftrightarrow \tau_6$	η	54.5	30.4	15.1
	τ_3	46.8	29.0	24.2
	τ_6	49.9	26.7	23.4
U_1: 930 °C	η	52.7	33.2	14.1
$\eta + \tau_3 \leftrightarrow \tau_4 + \tau_6$	τ_3	46.4	28.5	25.1
	τ_4	27.0	~49.0	24.0
	τ_6	49.2	28.0	22.8
U_2: 910 °C	α_2	72.2	~1.0	26.8
$\tau_3 + \tau_6 \leftrightarrow \tau_4 + \alpha_2$	τ_3	44.8	28.7	26.5
	τ_4	26.8	~49.0	24.2
	τ_6	48.2	27.2	24.6
E_1: 870 °C	α_2	72.4	~1.0	26.6
$\tau_6 \leftrightarrow \eta + \alpha_2 + \tau_4$	η	52.9	34.0	13.1
	τ_4	27.2	~49.0	23.8
	τ_6	47.6	28.3	24.1

[a] Ni is approximate due to small amount of α_2 and τ_4 in most of samples.

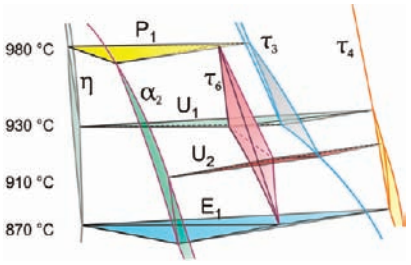

Figure 9. 3D-phase diagram for region of existence of τ_6-$Ti_2(Ti_{0.16}Ni_{0.43}Al_{0.41})_3$. Composition of equilibrium phases is available from Figure 5 and Table 7.

α_2-Ti_3Al, and the Laves phase $Ti(Ti,Ni,Al)_2$ (τ_3) and finally to derive a Schultz–Scheil diagram. Evaluations are summarized in a set of partial isothermal sections at 865, 900, 925, 950, 975 °C, in a subsolidus diagram (see Figure 6) and resulted in the Schultz–Scheil reaction scheme presented in Figure 7.

Alloys annealed at 1000 °C (Figure 8a1,b) show big grains of equilibrium phases ($\eta + \tau_3 + \tau_4$ and $\eta + \alpha_2 + \tau_3$, respectively) and little amount of a eutectic-like structure indicating that these alloys were close to the melting temperature. This observation agrees with data[10] on the existence of liquid in this part of the phase diagram at 1000 °C.

With decrease of temperature to 975 °C, alloys from the phase field $\eta + \alpha_2 + \tau_3$ undergo a phase transformation with formation of the new phase τ_6. Accordingly, we observe at this temperature three new phase tie-triangles $\eta + \tau_3 + \tau_6$, $\alpha_2 + \tau_3 + \tau_6$, and $\eta + \alpha_2 + \tau_6$ (Figure 8c,d,e) inferring the existence of the invariant reaction P_1, $\eta + \alpha_2 + \tau_3 \leftrightarrow \tau_6$, which was defined to occur at 980 ± 10 °C (Table 8, Figures 7and 9).

Alloys $\eta + \tau_3 + \tau_4$ (Figure 8a1) do not change phase composition up to 950 °C (Figure 8a2). However, the samples annealed at 925 °C for this triangle already reveal τ_6 (Figures 6d and 8f). Therefore, a temperature of 930 °C was assigned to the invariant equilibrium U_1, $\eta + \tau_3 \leftrightarrow \tau_4 + \tau_6$, that is responsible for the observed change of phase equilibria. The three phase field $\tau_3 + \tau_4 + \tau_6$ that forms during this reaction is very narrow and exists in a small temperature range. Attempts to quench any equilibrated three phase sample from this field were unsuccessful and resulted in four-phase microstructures containing α_2, τ_3, τ_4, and η (Figure 6d). However, from the interpretation of all other phase triangles at 925 °C (Figure 6d), it is obvious that also the equilibrium $\tau_3 + \tau_4 + \tau_6$ exists. Further decrease of annealing temperature to 910 °C results in different phase equilibria, and τ_6 does not participate anymore in equilibria with τ_3 (Figures 6e and 8h, i). Phase equilibria observed, $\alpha_2 + \tau_4 + \tau_6$ (Figure 8h) and $\alpha_2 + \tau_3 + \tau_4$ (Figure 8i), result from the transition reaction U_2 at 910 °C: $\tau_3 + \tau_6 \leftrightarrow \tau_4 + \alpha_2$. The τ_6-phase decomposes at 870 °C in a eutectoid invariant reaction $\tau_6 \leftrightarrow \eta$–$(Ti,Al)_2Ni + \alpha_2 + \tau_4$ with the formation of subsequent phase field $\eta + \alpha_2 + \tau_4$ at lower temperatures (Figure 8j). Consequently, we cannot confirm the reaction η-$(Ti,Al)_2Ni + \tau_3 \leftrightarrow \alpha_2 + \tau_4$ at 876 ± 2 °C claimed by Schuster et al.,[10] who did not consider the data[17] on the existence of τ_6. A significant discrepancy also occurs on the extension of the τ_3 phase field at 900 °C, which was reported[10] to exist at a Ti content higher than 50 at. %, while the maximum solubility of 47 at. % Ti at 1000 °C[10] agrees well with our data (Figure 5).

A three-dimensional view of the phase diagram for the composition–temperature range investigated is shown in Figure 9.

It is worth noticing that τ_6 is not reported yet in the literature in any homologous system of Ti–Ni–Al like Zr–Ni–Al,[30] Hf–Ni–Al,[31] Ti–Pd–Al,[32] Ti–Co–Al,[33] Ti–Ni–Si,[34] etc.

4. CONCLUSION

The crystal structure of τ_6-$Ti_2(Ti_{0.16}Ni_{0.43}Al_{0.41})_3$ was solved via combined evaluation of XRD and NPD data. τ_6-$Ti_2(Ti,Ni,Al)_3$ was found to be an isotypic variant of the $V_2(Co_{0.57}Si_{0.43})_3$-type. The structure is composed of slabs of the $MgZn_2$-Laves type and slabs of the Zr_4Al_3-type forming a tetrahedrally close-packed Frank–Kasper structure. Phase relations in the temperature interval from 1000 to 865 °C were determined for a set of isothermal sections at 865, 900, 925, 950, and 975 °C and in a subsolidus diagram. A Schultz–Scheil reaction scheme has been derived which comprises four isothermal reactions all involving the new phase τ_6. The τ_6 phase forms on cooling in a peritectoid reaction at 980 °C, η-$(Ti,Al)_2Ni + \tau_3 + \alpha_2 \leftrightarrow \tau_6$, and decomposes on cooling in a eutectoid reaction at about 870 °C, $\tau_6 \leftrightarrow \eta$-$(Ti,Al)_2Ni + \tau_4 + \alpha_2$. Atomic positions and distribution of Al in η-$(Ti,Al)_2Ni$ were evaluated from X-ray single crystal data.

AUTHOR INFORMATION

Corresponding Author

*E-mail: peter.franz.rogl@univie.ac.at.

ACKNOWLEDGMENT

The research reported herein was supported by the Higher Education Commission of Pakistan (HEC) under the scholarship scheme "PhD in Natural and Basic Sciences from Austria" and the Austrian OEAD.

DEDICATION

This paper is dedicated to Dr. Hans Leo Lukas on the occasion of his 80th birthday.

REFERENCES

(1) Tetsui, T.; Miura, T. *Tech. Rev.—Mitsubishi Heavy Ind.* **2002**, *39* (1), 268–271.

(2) Raman, A.; Schubert, K. *Z. Metallkd.* **1965**, *56*, 99–104.

(3) Markiv, V. Y.; Burnashova, V. V.; Ryabov, V. R. *Metallofizika* **1973**, *46*, 103–110.
(4) Nash, P.; Liang, W. W. *Metall. Trans.* **1985**, *16/A*, 319–322.
(5) Mazdiyasni, S.; Miracle, D. B.; Dimiduk, D. M.; Mendiratta, M. G.; Subramanian, P. R. *Scr. Metall.* **1989**, *23*, 327–331.
(6) Xu, H. H.; Jin, Z. *Trans. Nonferrous Met. Soc. China* **1997**, *7*, 24–29.
(7) Huneau, B.; Rogl, P.; Zeng, K.; Schmid-Fetzer, R.; Bohn, M.; Bauer, J. *Intermetallics* **1999**, *7*, 1337–1345.
(8) Zeng, K.; Schmid-Fetzer, R.; Huneau, B.; Rogl, P.; Bauer, J. *Intermetallics* **1999**, *7*, 1347–1359.
(9) Ding, J. J.; Rogl, P.; Schmidt, H. *J. Alloys Compd.* **2001**, *317−318*, 379–384.
(10) Schuster, J. C.; Pan, Z.; Liu, S.; Weitzer, F.; Du, Y. *Intermetallics* **2007**, *15*, 1257–1267.
(11) Raghavan, V. *Journal of Phase Equilibria and Diffusion* **2005**, *26*, 268–272.
(12) Raghavan, V. *J. Phase Equilib. Diffus.* **2010**, *31*, 55–56.
(13) Schuster, J. C. *Intermetallics* **2006**, *14/(10−11)*, 1304–1311.
(14) Dupin, N. Ph.D. Thesis, Institut National Polytechnique Grenoble, France, 1995.
(15) Bursik, J.; Broz, P. *Intermetallics* **2009**, *17*, 591–595.
(16) Khan, A. U.; Yan, X.; Rogl, P.; Saccone, A. *Intermetallics* **2009**, *17/12*, 1000–1006.
(17) Grytsiv, A.; Chen, X.-Q.; Witusiewicz, V. T.; Rogl, P.; Podloucky, R.; Pomjakushin, V.; Maccio, D.; Saccone, A.; Giester, G.; Sommer, F. Z. *Kristallografiya* **2006**, *221*, 334–348.
(18) Huneau, B.; Ding, J. J.; Rogl, P.; Bauer, J.; Ding, X. Y.; Bohn, M. *J. Solid State Chem.* **2000**, *155*, 71–77.
(19) *INCA Energy-300*; Oxford Instruments Analytical Ltd., Oxford, U.K., 2000.
(20) *Nonius Kappa CCD Program Package COLLECT, DENZO, SCALEPACK, SORTAV*; Nonius Delft: The Netherlands.
(21) Sheldrick, G. M. *SHELXL-97, Program for Crystal Structure Refinement*; University of Göttingen and National University of Ireland (Windows version by McArdle): Göttingen, Germany, and Galway, Ireland, 1997.
(22) Fischer, P.; Frey, G.; Koch, M.; Koennecke, M.; Pomjakushin, V.; Schefer, J.; Thut, R.; Schlumpf, N.; Buerge, R.; Greuter, U.; Bondt, S.; Berruyer, E. *Physica B* **2000**, *276−278*, 146.
(23) Roisnel, T.; Rodriguez-Carvajal, J. *Mater. Sci. Forum* **2001**, *118*, 378–381.
(24) Gelato, L. M.; Parthe, E. *J. Appl. Crystallogr.* **1987**, *20*, 139–143.
(25) Villars, P.; Cenzual, K. *Pearson's Crystal Data*; ASM International: Materials Park, OH; Release 2010/11.
(26) Krypyakevich, P. I.; Yarmolyuk, Y. P. *Dopov. Akad. Nauk. Ukr. RSR, Ser.* **1970**, *A 32*, 948–950.
(27) Hlukhyy, V.; Pöttgen, R. *Solid State Sci.* **2004**, *6/10*, 1175–1180.
(28) Cerny, R.; Renaudin, G.; Tokaychuk, Y.; Favre-Nicolin, V. Z. *Kristallografiya* **2006**, *23* (Suppl.), 411–416.
(29) *Gmelin Handbook of Inorganic and Organometallic Chemistry*; Typix, 1993; Vol. 1, p 169.
(30) Ghosh, G.; Effenberg G.; Ilyenko, S. *SpringerMaterials: The Landolt-Börnstein Database*; 2005; DOI: 10.1007/10915998_35.
(31) Raghavan, V. *J. Phase Equilib. Diffus.* **2009**, *30/1*, 64–66.
(32) Zaikina, O. V.; Khorujaya, V. G.; Pavlyuchkov, D.; Grushko, B.; Velikanova, T. Ya. *J. Alloys Compd.* **2011**, *509*, 43–51.
(33) Raghavan, V. *J. Phase Equilib. Diffus.* **2005**, *26/2*, 175–177.
(34) *SpringerMaterials: The Landolt-Börnstein Database*; Lebrun, N., Effenberg, G., Ilyenko, S., Eds.; 1999; DOI: 10.1007/11008514_38, .